Simultaneous three-dimensional tracking of individual signals from multi-trap optical tweezers using fast and accurate photodiode detection

Dino Ott,[1] S. Nader S. Reihani,[1,2] and Lene B. Oddershede[1,*]

[1]*Niels Bohr Institute (NBI), University of Copenhagen, Blegdamsvej 17, DK-2100 Copenhagen, Denmark*
[2]*Physics Department, Sharif University of Technology, 11365-9161 Tehran, Iran*
[*]*oddershede@nbi.dk*

Abstract: Multiple-beam optical traps facilitate advanced trapping geometries and exciting discoveries. However, the increased manipulation capabilities come at the price of more challenging position and force detection. Due to unrivaled bandwidth and resolution, photodiode based detection is preferred over camera based detection in most single/dual-beam optical traps assays. However, it has not been trivial to implement photodiode based detection for multiple-beam optical traps. Here, we present a simple and efficient method based on spatial filtering for parallel photodiode detection of multiple traps. The technique enables fast and accurate 3D force and distance detection of multiple objects simultaneously manipulated by multiple-beam optical tweezers.

© 2014 Optical Society of America

OCIS codes: (350.4855) Optical tweezers or optical manipulation; (120.1880) Detection; (230.5170) Photodiodes; (070.6110) Spatial filtering; (090.0090) Holography; (140.7010) Laser trapping; (170.4520) Optical confinement and manipulation.

References and links

1. R. T. Dame, M. C. Noom, and G. J. L. Wuite, "Bacterial chromatin organization by H-NS protein unravelled using dual DNA manipulation," Nature **444**, 387–390 (2006).
2. M. Noom, B. V. D. Broek, J. van Mameren, and G. J. L. Wuite, "Visualizing single DNA-bound proteins using DNA as a scanning probe," Nat. Methods **4**, 1031–1036 (2007).
3. H. Kress, J.-G. Park, C. O. Mejean, J. D. Forster, J. Park, S. S. Walse, Y. Zhang, D. Wu, O. D. Weiner, T. M. Fahmy, and E. R. Dufresne, "Cell stimulation with optically manipulated microsources," Nat. Methods **6**, 905–909 (2009).
4. M. Polin, D. Grier, and S. Quake, "Anomalous vibrational dispersion in holographically trapped colloidal arrays," Phys. Rev. Lett. **96**, 088101 (2006).
5. M. Padgett and R. Di Leonardo, "Holographic optical tweezers and their relevance to lab on chip devices," Lab Chip **11**, 1196–1205 (2011).
6. T. Čižmár, M. Mazilu, and K. Dholakia, "In situ wavefront correction and its application to micromanipulation," Nature Photon. **4**, 388–394 (2010).
7. J. Liesener, M. Reicherter, T. Haist, and H. J. Tiziani, "Multi-functional optical tweezers using computer-generated holograms," Opt. Commun. **185**, 77–82 (2000).
8. E. R. Dufresne, G. C. Spalding, M. T. Dearing, S. A. Sheets, and D. G. Grier, "Computer-generated holographic optical tweezer arrays," Rev. Sci. Instrum. **72**, 1810 (2001).
9. J. Curtis, B. Koss, and D. Grier, "Dynamic holographic optical tweezers," Opt. Commun. **207**, 169–175 (2002).
10. C. Schmitz, J. Spatz, and J. Curtis, "High-precision steering of multiple holographic optical traps," Opt. Express **13**, 8678–8685 (2005).

#220874 - $15.00 USD Received 12 Aug 2014; accepted 7 Sep 2014; published 19 Sep 2014

11. K. C. Neuman and S. M. Block, "Optical trapping," Rev. Sci. Instrum. **75**, 2787–2809 (2004).
12. K. Visscher, S. Gross, and S. Block, "Construction of multiple-beam optical traps with nanometer-resolution position sensing," IEEE J. Sel. Top. Quant. Electron. **2**, 1066–1076 (1996).
13. F. Gittes and C. F. Schmidt, "Interference model for back-focal-plane displacement detection in optical tweezers," Opt. Lett. **23**, 7–9 (1998).
14. A. Pralle, M. Prummer, E. L. Florin, E. H. Stelzer, and J. K. Hörber, "Three-dimensional high-resolution particle tracking for optical tweezers by forward scattered light," Microsc. Res. Tech. **44**, 378–386 (1999).
15. S. Keen, J. Leach, G. Gibson, and M. J. Padgett, "Comparison of a high-speed camera and a quadrant detector for measuring displacements in optical tweezers," J. Opt. A: Pure Appl. Opt. **9**, 264–266 (2007).
16. J. R. Moffitt, Y. R. Chemla, S. B. Smith, and C. Bustamante, "Recent advances in optical tweezers," Annu. Rev. Biochem. **77**, 205–228 (2008).
17. C. Pacoret and S. Régnier, "Invited article: a review of haptic optical tweezers for an interactive microworld exploration," Rev. Sci. Instrum. **84**, 081301 (2013).
18. R. Bowman, G. Gibson, and M. Padgett, "Particle tracking stereomicroscopy in optical tweezers: control of trap shape," Opt. Express **18**, 11785–11790 (2010).
19. R. F. Hay, G. M. Gibson, M. P. Lee, M. J. Padgett, and D. B. Phillips, "Four-directional stereo-microscopy for 3D particle tracking with real-time error evaluation," Opt. Express **22**, 18662–18667 (2014).
20. D. B. Conkey, R. P. Trivedi, S. R. P. Pavani, I. I. Smalyukh, and R. Piestun, "Three-dimensional parallel particle manipulation and tracking by integrating holographic optical tweezers and engineered point spread functions," Opt. Express **19**, 3835–3842 (2011).
21. S. Lee, Y. Roichman, G. Yi, S.-H. Kim, S.-M. Yang, A. van Blaaderen, P. van Oostrum, and D. G. Grier, "Characterizing and tracking single colloidal particles with video holographic microscopy," Opt. Express **15**, 18275–18282 (2007).
22. F. Cheong, B. Sun, R. Dreyfus, J. Amato-Grill, K. Xiao, L. Dixon, and D. G. Grier, "Flow visualization and flow cytometry with holographic video microscopy," Opt. Express **17**, 13071–13079 (2009).
23. F. Cheong, B. Krishnatreya, and D. Grier, "Strategies for three-dimensional particle tracking with holographic video microscopy," Opt. Express **18**, 13563–13573 (2010).
24. L. Miccio, P. Memmolo, F. Merola, S. Fusco, V. Embrione, A. Paciello, M. Ventre, P. A. Netti, and P. Ferraro, "Particle tracking by full-field complex wavefront subtraction in digital holography microscopy," Lab Chip **14**, 1129–1134 (2014).
25. R. Di Leonardo, S. Keen, J. Leach, C. Saunter, G. Love, G. Ruocco, and M. Padgett, "Eigenmodes of a hydrodynamically coupled micron-size multiple-particle ring," Phys. Rev. E **76**, 061402 (2007).
26. G. M. Gibson, J. Leach, S. Keen, A. J. Wright, and M. J. Padgett, "Measuring the accuracy of particle position and force in optical tweezers using high-speed video microscopy," Opt. Express **16**, 14561–14570 (2008).
27. M. Towrie, S. W. Botchway, A. Clark, E. Freeman, R. Halsall, A. W. Parker, M. Prydderch, R. Turchetta, A. D. Ward, and M. R. Pollard, "Dynamic position and force measurement for multiple optically trapped particles using a high-speed active pixel sensor," Rev. Sci. Instrum. **80**, 103704 (2009).
28. O. Otto, F. Czerwinski, J. L. Gornall, G. Stober, L. B. Oddershede, R. Seidel, and U. F. Keyser, "Real-time particle tracking at 10,000 fps using optical fiber illumination," Opt. Express **18**, 22722–22733 (2010).
29. R. Huang, I. Chavez, K. M. Taute, B. Lukić, S. Jeney, M. G. Raizen, and E.-L. Florin, "Direct observation of the full transition from ballistic to diffusive Brownian motion in a liquid," Nature Phys. **7**, 576–580 (2011).
30. F. Marsà, A. Farré, E. Martín-Badosa, and M. Montes-Usategui, "Holographic optical tweezers combined with back-focal-plane displacement detection," Opt. Express **21**, 30282–30294 (2013).
31. W. H. Guilford, J. A. Tournas, D. Dascalu, and D. S. Watson, "Creating multiple time-shared laser traps with simultaneous displacement detection using digital signal processing hardware," Anal. Biochem. **326**, 153–166 (2004).
32. D. Ruh, B. Tränkle, and A. Rohrbach, "Fast parallel interferometric 3D tracking of numerous optically trapped particles and their hydrodynamic interaction," Opt. Express **19**, 21627–21642 (2011).
33. D. Ott, S. N. S. Reihani, L. B. Oddershede, "Crosstalk elimination in the detection of dual-beam optical tweezers by spatial filtering," Rev. Sci. Instrum. **85**, 053108 (2014).
34. E. R. Dufresne and D. G. Grier, "Optical tweezer arrays and optical substrates created with diffractive optics," Rev. Sci. Instrum. **69**, 1974 (1998).
35. P. M. Hansen, I. M. Tolić-Nørrelykke, H. Flyvbjerg, and K. Berg-Sørensen, "tweezercalib 2.0: faster version of MatLab package for precise calibration of optical tweezers," Comput. Phys. Commun. **174**, 518–520 (2006).
36. K. Berg-Sørensen, L. Oddershede, E.-L. Florin, and H. Flyvbjerg, "Unintended filtering in a typical photodiode detection system for optical tweezers," J. Appl. Phys. **93**, 3167 (2003).
37. A. Rohrbach, "Stiffness of optical traps: quantitative agreement between experiment and electromagnetic theory," Phys. Rev. Lett. **95**, 168102 (2005).
38. W. M. Lee, P. J. Reece, R. F. Marchington, N. K. Metzger, and K. Dholakia, "Construction and calibration of an optical trap on a fluorescence optical microscope," Nat. Protoc. **2**, 3226–3238 (2007).
39. J. K. Dreyer, K. Berg-Sørensen, and L. Oddershede, "Improved axial position detection in optical tweezers measurements," Appl. Opt. **43**, 1991–1995 (2004).

#220874 - $15.00 USD Received 12 Aug 2014; accepted 7 Sep 2014; published 19 Sep 2014
(C) 2014 OSA

40. R. L. Eriksen, P. C. Mogensen, and J. Glückstad, "Multiple-beam optical tweezers generated by the generalized phase-contrast method," Opt. Lett. **27**, 267–269 (2002).

1. Introduction

Multiple trap optical tweezers have been instrumental in exciting studies of, e.g., chromatin organization by DNA-structuring proteins [1, 2], the role of cell polarisation in chemotaxis [3], and many-body dynamics of hydrodynamical coupled particles [4], also they have a high potential for lab-on-a-chip devices [5]. Boosted by the rapid advances of holographic light shaping techniques within the fields of imaging and optical fiber communication [6], significant progress has been made to dynamically generate advanced optical trapping landscapes [7–10] and holographic optical tweezers (HOTs) are one of the most common techniques for creating multiple traps. Beside the possibility to manipulate and actively perturb a system of interest with extrinsic forces, the ability to precisely measure the response of the investigated system like, e.g., a living cell reacting to external mechanical stimuli, is of utmost interest, as it allows for quantitative investigations of the underlying (bio-)physical mechanisms at play. However, the development of suitable detection methods, to accurately measure forces and displacements of multiple trapped particles, has proven quite challenging.

For force and distance detection in optical traps, the two prevalent detection schemes are camera or photodiode based [11]. Interferometric photodiode based detection is typically used for single or dual traps due to its unrivaled spatial and temporal resolution [12]; this method allows for extraction of displacements and forces at bandwidths of hundreds of kHz with sub-nanometer and piconewton accuracy in all three dimensions [13, 14]. The method's incompatibility with the detection of multiple traps presents a major drawback, though, and has limited its use in conjunction with holographic optical tweezers.

Therefore, camera-based detection has been widely used for multiple tweezers. However, in comparison to photodiode detection, this implies reduced spatial and temporal resolution, offline data processing, higher costs and limited axial detection capability. On the positive side, camera based detection easily allows for monitoring many particles in parallel [15–17]. To improve the axial detection capabilities of multi-trap camera based imaging, stereoscopic imaging [18, 19] and point spread function engineering [20] have been presented. Furthermore, holographic particle tracking methods [21–24], relying on analyzing recorded interference patterns, created under coherent illumination, have been demonstrated to achieve nanometer-scale resolution in both the lateral and axial directions. However, the downside of all these techniques is a low temporal resolution and a rather challenging and computationally demanding data analysis [5]. The speed of camera detection is ultimately limited by the number of detected photons per recorded image, resulting in a low signal-to-noise ratio for high frame rates. Pushing the boundaries by sophisticated "smart cameras" with integrated image processing [25–27] and by specialized high radiance illumination [28], camera-based solutions can reach frame rates of tens of kHz which is comparable to the performance of standard QPD detection. However, photodiodes can operate at significantly higher bandwidths, as used, e.g., for measuring Brownian particle movement with a stunning bandwidth of 75 MHz [29].

Photodiode-based detection for multiple-beam optical traps is a worthwhile challenge as it opens the door to ultra-fast and precise force and distance measurements by multiple tweezers [16, 30]. To this end, one solution has been to create one of the multiple traps with a polarization that is orthogonal to the polarization of the additional traps; the signal from the 'orthogonal trap' can then be separated out using polarization optics and used for individual interferometric detection. However, the two available polarization states set a limitation on the maximal number of interferometrically detectable traps using this method [1, 2, 30]. An alternative method is to use a time-shared QPD detection [31, 32], i.e., a sequential trap detection, which trades a

#220874 - $15.00 USD Received 12 Aug 2014; accepted 7 Sep 2014; published 19 Sep 2014
(C) 2014 OSA

lowered sample rate for additional detectable traps.

Here, we present and demonstrate a new detection method for multi-beam optical tweezers which enables simultaneous, fast and accurate detection of multiple optical traps by photodiodes. The method is low-cost and easy to implement in existing setups. It is based on spatial filtering and, as shown for dual traps [33], allows to exclusively detect the signal from any individual trap of interest. The signal separation is achieved by selective light transmission using a pinhole positioned in a plane optically conjugate to the sample plane, where the trapping is performed. We show how to use this principle of spatial filtering in a simple, yet powerful, manner to perform parallel position and force measurements of multiple beads using photodiodes placed in the back-focal-plane of holographic optical tweezers. For each individual trap, we confirm that hallmarks of optical trapping as, e.g., the linear QPD detection range and the linear power dependency of the trap stiffness, remain valid.

2. Principle of signal separation

Interferometric detection schemes are based on capturing the interference pattern, created by the coherent superposition of un-scattered and forward-scattered light by the trapped object, using position sensing devices, e.g., quadrant photodiodes. Typically, the photodiodes are not positioned precisely at the back-focal-plane of the light-collecting condenser, instead, for optimal performance, one or multiple relay lenses are used for creating a scaled image of the interference pattern that fills the active region of the photodiode. Due to this additional imaging, an intermediate plane exists, which is optically conjugated with the sample plane. This can be advantageously exploited for signal selection, as illustrated in Fig. 1. In this conjugate plane, an image of the sample plane is formed, which is a replication of the optical traps in the sample plane, modified according to the optical transfer function of the lenses in-between. Accurately positioning a pinhole in this plane allows for the selective transmission of a chosen trap of interest for subsequent individual interferometric detection. For dual-beam optical traps, it was shown that a similar spatial filtering rejects the signal from the adjacent trap and crosstalk levels of less than 5% could routinely be achieved (although, dependent, e.g., on pinhole size); combining spatial filtering with polarisation-based filtering provided crosstalk levels less than 0.2% for dual traps with orthogonal polarization [33].

3. Experiment

3.1. Optical setup

Holographic optical tweezers were implemented through the back port of an inverted microscope (Leica DM IRBE), the setup is sketched in Fig. 1. An expanded Gaussian-shaped laser beam (1064nm CW Nd:YVO_4 laser, Spectra Physics J20I-BL-106C-02), with an initially flat wavefront profile, was phase-modulated by a diffractive optical element (HOLO/OR LTD., MS-231-I-Y-A). The plane of the diffractive optical element was optically conjugated with the back-focal-plane of the objective using a 1:1-telescope, to ensure an effective conversion of the phase-modulation to the intensity distribution in the focal plane of the objective (63X, NA=1.2, water immersion, Leica HCX PL APO W CORR CS) [34]. Two #1.5 glass cover slips, sandwiched on top of each other and separated by double sided sticky tape, formed a perfusion sample chamber, 80μm in thickness. The chamber contained polystyrene beads with a mean diameter of 0.96μm (PS03N/9396, Bangs Laboratories), dispersed in Millipore water. All trapping experiments were conducted with the trapping plane far from any surfaces, i.e., 15μm above the bottom of the chamber. An oil immersion condenser (NA = 1.4, Leica S1 551004), opposing the microscope objective, was used for light collection. The back-focal-plane of the condenser was imaged onto a QPD (Si-PIN photodiode, Hamamatsu S5981) using a relay lens

#220874 - $15.00 USD Received 12 Aug 2014; accepted 7 Sep 2014; published 19 Sep 2014
(C) 2014 OSA

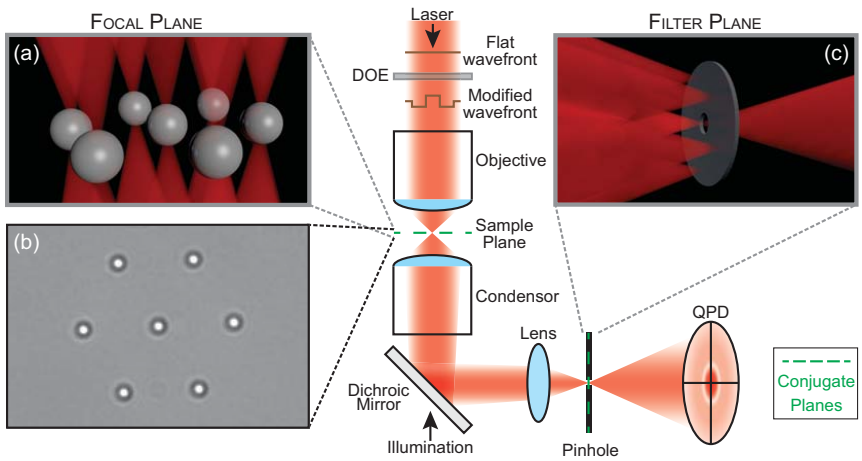

Fig. 1. Illustration of the detection method. A diffractive optical element (DOE) is used to modify the wavefront of the trapping beam to holographically generate a complex trapping landscape in the sample plane, e.g., a hexagonal arrangement of seven optical traps. By means of a relay lens, the back-focal-plane of the condenser is imaged onto a quadrant photodiode (QPD). A pinhole, placed in the intermediate plane, which is optically conjugate to the sample plane, selects a single trap for transmission and detection. Inset a: Visualization of trapping geometry in the sample plane. Inset b: Top view captured by camera, bead diameter = 1 μm. Inset c: Visualization of spatial filtering in the conjugate plane.

with a focal length of $5cm$.

To track a single particle at a time we added a pinhole (diameter $15\mu m$, Thorlabs P15S) in the optical plane where an image of the sample was formed. Micro-positioning (Thorlabs, ST1XY-D) of the pinhole allowed for precise alignment of the pinhole with a specific trap of interest. The signal from the photodiode was digitized using an A/D card after amplification by a low-noise amplifier. The total signal of all four quadrants on the QPD was used as a read-out of the transmitted intensity while aligning the pinhole. Good alignment could be achieved by maximizing the transmitted signal and verifying that a Lorentzian power spectrum could be measured when a bead was trapped in the trap of interest. This optimization process took 5 minutes to do 'by hand', however, this part of the experimentation could be optimized by a feedback mechanism between the read-out on the photodiode and an automatized positioning of the pinhole.

To track multiple (i.e., more than two, here proven for three) particles simultaneously, we split the laser beam into three beams keeping the polarization of the original laser beam in each of the multiple daughter-beams. This was done by inserting two beam splitters ($10mm$, Thorlabs) after the relay lens. In each of the multiple optical paths we added a pinhole in the optical plane conjugate to the sample plane. Each pinhole was mounted on a separate micro-positioner (Thorlabs, ST1XY-D). This allowed for precise alignment of the pinholes with each of the traps of interest. The optimal pinhole size and the required precision in pinhole position depend on the magnification produced by the relay lens. For the multi-particle tracking measurement we used a relay lens with focal length of $7.5cm$, which magnified the waist of each trap and, most importantly, provided a larger space for positioning of the optical elements. In our case, the inter-trap distance between two adjacent traps in the 7-trap system was measured to be $\sim 40\mu m$ in the image plane. Therefore, we used pinholes with diameters of $30\mu m$ and $50\mu m$. The light

#220874 - $15.00 USD Received 12 Aug 2014; accepted 7 Sep 2014; published 19 Sep 2014
(C) 2014 OSA

passing through each of the pinholes was collected with a separate photodiode, all photodiodes being similar to the one described above, and the signals from each of the traps were treated in parallel.

Trap calibration via power spectral analysis was done as previously described [33] using a freely available Matlab program [35], that also includes corrections for the significant filtering effect of the photodiode [36], aliasing and other minor effects. Briefly, the 1D dynamics of a trapped bead, undergoing confined Brownian motion in a harmonic optical potential, can be described by the Langevin equation

$$m\ddot{x}(t) + \gamma\dot{x}(t) + \kappa x(t) = F_{\text{therm}}(t), \tag{1}$$

where x denotes the bead's time-dependent position, m its mass and γ its friction coefficient given by Stokes' law. The random and time-dependent force term $F_{\text{therm}}(t)$ accounts for the stochastic thermal collisions with the solvent molecules, and the strength of the harmonic optical trapping potential, $F_{trap} = \kappa x$, is characterized by the spring constant κ. The dynamics in the other two translational directions are equivalent to that described above, however, each with a different κ. The Langevin equation can be recast into a power spectrum, describing the bead's motion in the optical trap in terms of its frequency components. The sampled power spectra will vary from experiment to experiment due to the stochastic character of $F_{\text{therm}}(t)$. However, the theoretically predicted power spectrum of the Langevin equation, $P(f)$, which is simply the expectation value of the experimental power spectrum, $P_{\text{exp}}(f)$, can be expressed as

$$P(f) = \left\langle P_{\text{exp}}(f) \right\rangle = \frac{A}{f_{\text{c}}^2 + f^2}. \tag{2}$$

Here, f_c is the corner frequency which is defined as $\kappa = 2\pi\gamma f_{\text{c}}$ and A is a constant that carries information about the conversion of the recorded QPD voltage signal to bead displacements in metric units, see details in [33].

3.2. Experimental results

A diffractive optical element created seven optical traps arranged as in a hexagonal lattice, i.e., one central trap was surrounded by a hexagon of traps. The distance between neighboring traps (see Fig. 1(b)) was measured to be 6.7μm in the sample.

To examine the performance of the spatial filtering detection method in a multi-trap system, we selected the central trap by positioning the pinhole so that only the light from the central trap was passed onto the photodiode and all other traps were blocked. As illustrated in Figs. 2(a)–2(c), we compared the trap characteristics obtained in three configurations: Fig. 2(a) The situation, when only the trap of interest contained a trapped bead; Fig. 2(b) the situation, when all seven traps contained trapped beads; and Fig. 2(c) the situation, when the surrounding six traps contained beads, while the trap of interest was left empty. By comparing the power spectra from the situations of Figs. 2(a) and 2(b), shown by purple squares and green circles, respectively, in Fig. 2(d), it is clear that the two situations yield power spectra that are indistinguishable by eye. The full lines in Fig. 2(d) show the fit of a Lorentzian power spectrum to the data. These fits returned corner frequencies, f_c, that, within the error bars, were identical for situations of Figs. 2(a) and 2(b). Also, both of these situations yielded power spectra distinctly different from that of an empty central trap (shown with orange triangles in Fig. 2(d)), which had a signal that was orders of magnitude lower. Hence, the method allows for individual detection of the trap of interest and efficiently rejects the signal from the remaining traps.

The desired information is knowledge of the distances travelled by the bead and the forces exerted on the bead by the trap. Therefore, an important step is the determination of the conversion factor, which mediates conversion from the measured QPD signals in volts to distance

#220874 - $15.00 USD Received 12 Aug 2014; accepted 7 Sep 2014; published 19 Sep 2014
(C) 2014 OSA

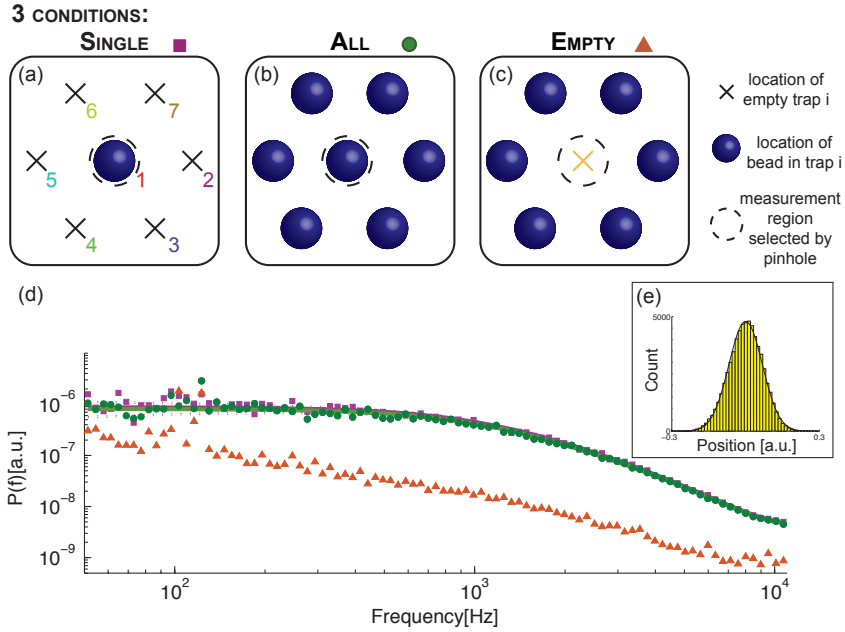

Fig. 2. Examination of spatial filtering in a multi-trap setup. a)–c) Illustrations of the three different experimental conditions, the pinhole allows light from the central trap to be passed on to the photodiode. d) Overlay of the measured power spectra for the situations shown in a) (purple squares), b) (green circles), and c) (orange triangles). Solid lines are fits to the experimental data for situations a) (purple) and b) (green) using the calibration program from Ref. [35] (the fitting range was 120Hz to 11kHz). Within the error bars (dashed lines) the two fitted power spectra overlap. The signal levels of an empty trap of interest (orange triangles) are orders of magnitude lower than for a full trap of interest. e) Position histogram of a trapped particle overlayed by a fit based on the theoretically expected Gaussian distribution.

measured in metric units. For easy conversion, it is convenient if one utilized a range where there is a linear relation between the QPD voltage signal and the actual distance travelled by the bead. This relation can be investigated by recording the QPD signals while scanning a bead that is immobilized on a cover slip through the focal region of the optical trap. The insets of Figs. 3(a) and 3(b) show that, also with the pinhole inserted, there does exist a wide range with a linear relation between the QPD voltage signal and the distance travelled by the bead (right insets) and that the linear detection in one lateral direction, in a certain region, is essentially independent on the other lateral direction (left insets). Knowledge of the conversion factors in all three dimensions thus allows for extraction of x, y and z in metric units.

A linear relation between the power of the trapping beam and the trap stiffness, κ is a hallmark of optical trapping. Figures 3(a) and 3(b) show κ as a function of laser power in the trap in the lateral x and y directions, respectively. The graphs show the result of a total of 3780 recorded and analyzed bead trajectories and confirm the expected linear dependency of κ versus power for all seven traps. With knowledge of x (or y) and the corresponding κ, the force exerted on the particle can be found and the calibration is complete.

#220874 - $15.00 USD Received 12 Aug 2014; accepted 7 Sep 2014; published 19 Sep 2014
(C) 2014 OSA

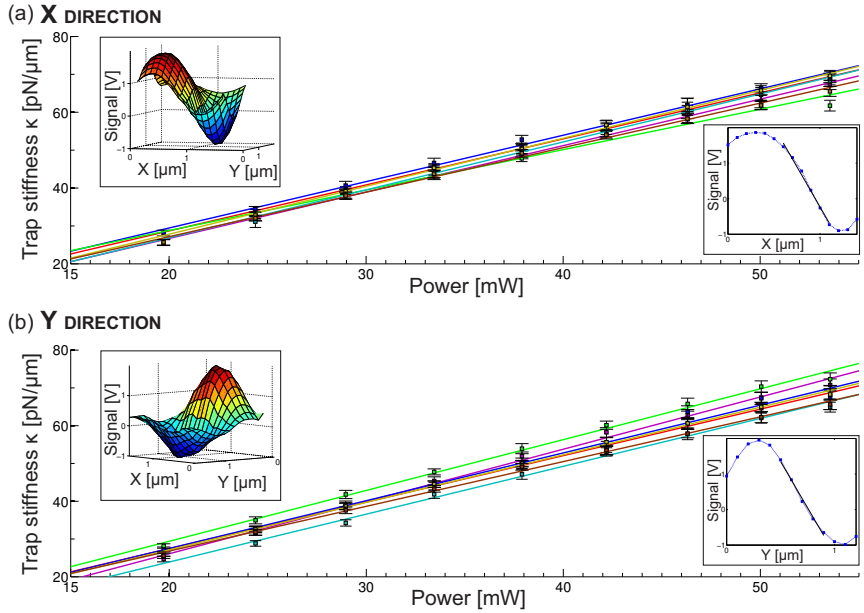

Fig. 3. Lateral force and displacement detection. a) The main graph shows the linear dependency of the trap stiffness versus laser power in the *x*-direction for all seven traps, the mean and one standard deviation of the measurements (N=30 per data point) are drawn in black. Full lines (color-coding according to Fig. 2(a)) are linear ordinary least square fits ($R^2 > 0.97$) to the data originating from each trap. The abscissa values denote the power of a single trap in the focal plane. Lower right inset: QPD voltage signal as a function of distance travelled by the bead in the *x*-direction. Upper left inset: Two-dimensional conversion factor scan, showing the dependency of the QPD voltage signal as function of both the *x*- and *y*-directions. b) Same as a), but for the Y-direction.

According to the DOE manufacturer, the total laser power reaching the focal plane is distributed equally between the seven focal points, with a total efficiency of 77% and a relative difference of maximal 5%. The power dependency of the spring constants, i.e., the slopes in Fig. 3, of the seven traps were measured to be $(1.205 \pm 0.069)\frac{\mathrm{pN}}{\mu\mathrm{m\ mW}}$ for the x-direction and $(1.276 \pm 0.067)\frac{\mathrm{pN}}{\mu\mathrm{m\ mW}}$ for the y-direction which is in fine agreement with typical values, e.g., from traps based on a single laser beam [37, 38].

As it is sometimes necessary to be able to perform quantitative measurements of force and distance in the axial direction, we also demonstrated the applicability of the method in the axial direction. The setup was still as shown as in Fig. 1 and, by restricting the aperture of the condenser, we optimized the dependency of the summed signal of the four QPD quadrants on the axial position of the trapped bead [39]. In this way, power spectra of the axial motion of the trapped beads were obtained. As shown in Fig. 4, even with the pinhole inserted, the axial direction yielded a linear relation between the QPD voltage signal and the distance travelled by the bead, the positions visited by the trapped bead yielded a Gaussian distribution, and the power spectrum had the expected Lorentzian shape. The axial spring constant, κ_z, was approximately 1/3 of the lateral spring constants, as is typical for optical traps. In our experiment, all traps had their focus in the same axial plane as they were created by a diffractive optical element. If, however, the axial foci of the traps were axially displaced from each other, as possible, e.g., by using the generalized phase contrast method [40], it might be important to perform a

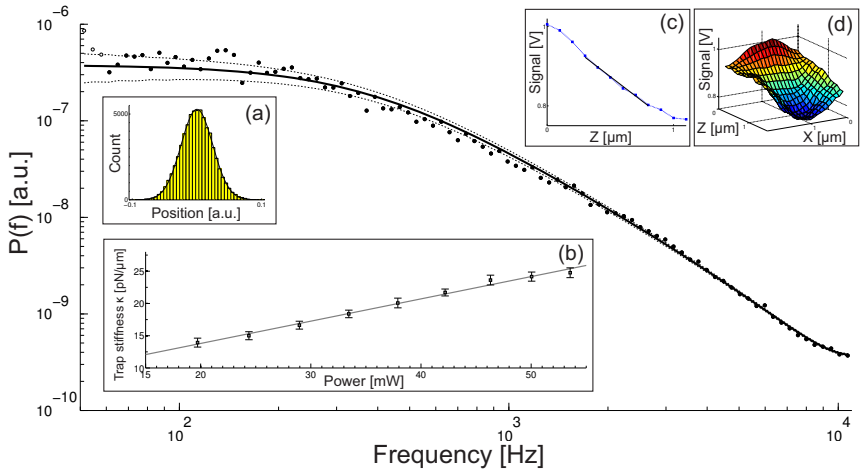

Fig. 4. Axial detection. The main graph shows the experimental axial power spectrum fitted by a Lorentzian function. Insets: a) Histogram of the axial displacement of a trapped bead. b) The axial spring constant as a function of laser power in the trap. The linear fit ($R^2 > 0.97$) has a slope of $0.345 \frac{\text{pN}}{\mu\text{m mW}}$. c) The total QPD signal as a function of the bead's axial displacement. d) Two-dimensional scan of the total QPD signal for XZ-displacement. As expected, around the equilibrium position, the total signal depends mainly on the axial position, while being nearly insensitive to lateral displacement in *x*-direction.

spatial filtering also in the axial direction. The problem with axial trap displacements is that if one trap, say the central one, is displaced upstream of the optical path (compared to the rest of the traps) there is a chance that some of the marginal rays of the central trap reach the other focal spots and give rise to a significant amount of crosstalk. This effect gives a maximum of the advisable axial distance between traps while employing axial photodiode detection, even if spatial filtering is performed. This maximum advisable distance depends on the NA of the converging optics and on the inter-trap distance. The lower the NA and the larger the inter-trap distance, the longer the advisable axial separation. In our case, if we would have been able to axially displace our traps, we estimate that the advisable axial separation distance would have been $\sim 10\mu m$.

Above we demonstrated the applicability of the spatial filtering method to detect a single trap of multiple-beam optical tweezers. However, the method is equally applicable to detect multiple particles within a multiple-beam optical trap simultaneously. To demonstrate photodiode detection of multiple (more than two) traps of arbitrary polarization, we performed a series of experiments where we simultaneously monitored three traps (the number of traps was only limited by the number of available photodiodes and low-noise amplifiers). We arbitrarily chose to monitor traps number 1, 2, and 4 (the numbering of the traps is visible in Fig. 2(a)), but any of the traps could have been chosen. As detailed under 'Optical setup' (Section 3.1) and visualized in Fig. 5(a), we used two beamsplitters to make three copies of the laser beams after the relay lens, inserted three pinholes, one for each beam (in a plane conjugate to the sample plane), and imaged each beam on one photodiode. In the experiments, we first tracked an individual bead that was trapped by either trap 1, trap 2, or trap 4. Figure 5(b) (first row) shows the corresponding power spectra measured in the three traps and Table 1 gives the corresponding lateral and axial corner frequencies for pinhole sizes of 30μm and 50μm, respectively. The two lateral directions were very similar, therefore only the *x* direction is given in the table. These results show a clear Lorentzian power spectrum of the occupied trap and a non-Lorentzian noisy

#220874 - $15.00 USD Received 12 Aug 2014; accepted 7 Sep 2014; published 19 Sep 2014
(C) 2014 OSA

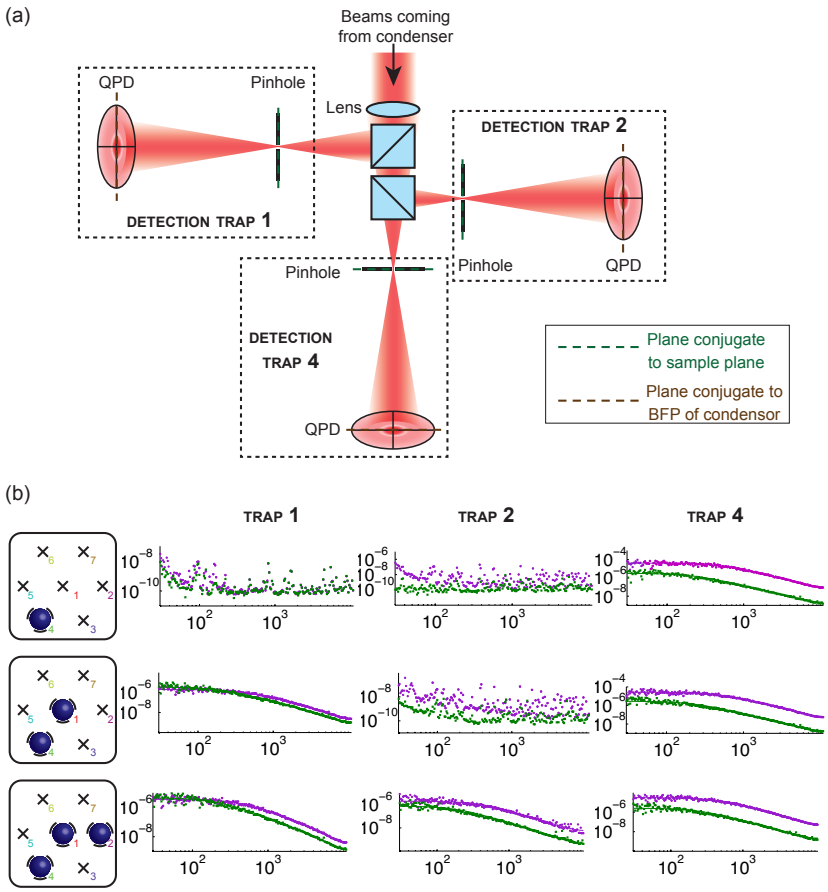

Fig. 5. Simultaneous detection of multiple beads occupying multiple traps. a) Schematic of how the detection part of the setup was modified in order to track three trapped beads simultaneously using photodiodes. b) The left schematics show the occupancy of the traps during each of the three types of measurements. The right graphs show corresponding lateral (purple) and axial (green) power spectra. For these experiments the pinhole diameter was 30μm.

#220874 - $15.00 USD Received 12 Aug 2014; accepted 7 Sep 2014; published 19 Sep 2014
(C) 2014 OSA

Table 1. The measured corner frequencies from multiple traps detected simultaneously. The traps are numbered and filled as shown in Fig. 5(b). Experiments were done using pinholes with diameters of either 30μm (upper part of table) or 50μm (lower part of table). Each number denotes the average of 10 measurements and the error is given as one standard deviation. A '-' denotes that the trap was empty and the power spectrum non-Lorentzian.

30μm pinhole								
			Trap 1 (T1)		Trap 2 (T2)		Trap 4 (T4)	
occupancy			X	Z	X	Z	X	Z
T1	-	-	482±15	201±6	-	-	-	-
-	T2	-	-	-	480±18	215±6	-	-
-	-	T4	-	-	-	-	481±13	213±5
T1	T2	-	444±12	198±7	404±10	194±6	-	-
T1	-	T4	422±10	194±7	-	-	460±10	222±9
-	T2	T4	-	-	378±35	214±5	453±19	208±5
T1	T2	T4	436±10	196±6	478±18	199±7	444±13	220±9
50μm pinhole								
			Trap 1 (T1)		Trap 2 (T2)		Trap 4 (T4)	
occupancy			X	Z	X	Z	X	Z
T1	-	-	449±12	195±6	-	-	-	-
-	T2	-	-	-	433±14	210±9	-	-
-	-	T4	-	-	-	-	495±27	235±8
T1	T2	-	460±8	184±6	489±11	208±3	-	-
T1	-	T4	460±12	187±9	-	-	490±17	228±10
-	T2	T4	-	-	485±10	224±11	488±14	236±9
T1	T2	T4	463±15	188±4	473±9	223±6	490±8	225±9

low signal from the empty traps, as expected, thus confirming a separation of the signals. The obtained corner frequencies are quite similar for all three traps, which is to be expected as the power was distributed evenly between them and exactly the same bead was transferred from one trap to another. Second, we performed experiments with two traps occupied, the corresponding results are shown in the second row of Fig. 5(b) and in Table 1. Again, the power spectra look as expected and the corner frequencies are in good agreement, especially considering the fact that these were different beads (with individual diameters). Third, we performed an experiment with all three traps occupied simultaneously, the results are shown in the last row of Fig. 5(b) and in Table 1. Again, all power spectra were as expected and the corner frequencies were in good agreement, thus demonstrating the ability to use a photodiode to successfully track multiple particles in a multiple beam optical trap simultaneously.

Two pinhole sizes were employed in the simultaneous tracking of multiple beads, 30μm and 50μm. Judging from Table 1, these two pinhole sizes yielded quite similar results and both work fine for spatial filtering in the setup depicted in Fig. 5(a). Based on the results of Ref. [33], however, the smaller pinhole probably suppresses crosstalk slightly more efficient than the larger.

It is straightforward to extend this method to a larger number of traps. For this, one should simply split the beam into more daughter-beams and use one pinhole and one photodiode for each trap. It might be an advantage to use a relay lens with a larger focal length, as this would

#220874 - $15.00 USD Received 12 Aug 2014; accepted 7 Sep 2014; published 19 Sep 2014
(C) 2014 OSA

provide a larger physical space for the necessary optical elements and it would employ a larger distance between the traps in the filtering plane, thus allowing for the use of a larger pinhole and lowering the precision requirements during pinhole adjustments.

4. Conclusion

This novel spatial filtering technique allows for fast and precise photodiode based back-focal-plane detection of multiple-beam optical tweezers that are formed, e.g., by holographic techniques [9] or by generalized phase-contrast [40]. Spatial filtering enables a separation of signals originating from different traps and we verified its capability of detecting three-dimensional position and force. Using this method, the usual hallmarks of optical trapping, e.g., a linear relation between photodiode signal and distance travelled and a linear relation between the spring constant and the laser power, were confirmed. The technique is here demonstrated for tracking up to three beads simultaneously in lateral and axial directions. The separation of the signals is independent of the polarization of the laser beam and can easily be extended up to a large number of beads with the only practical limitation being the number of photodiodes available. If the detection technique would be highly parallelized, splitting the beam many times would result in a decreased signal-to-noise ratio and thus comes at the cost of reduced accuracy. The method here presented will allow multiple-tweezers based high-bandwidth investigations, e.g., of interactions of trapped networks of particles [25, 29] and will improve single molecule experiments that involve tracking of multiple tracers [1, 2].

Acknowledgments

The authors acknowledge financial support from the University of Copenhagen Excellence Program.